

# The Impact of Strain Gage Instrumentation on Localized Strain Responses in Asphalt Concrete Pavements

Hao Yin<sup>1+</sup>

**Abstract:** Reliable determination of pavement response to variable environmental and traffic conditions is essential for successful mechanistic design of asphalt concrete (AC) pavements. By measuring the responses directly, the assumptions and simplifications are not of concern. However, the introduction of the instrumentation into the pavement structure may itself inherently and significantly affect the pavement responses. This concern has led to questions about what is actually being measured by in-situ gages. When comparing measured and predicted responses, can one set of information be considered the “ground truth?” In this paper, the impact of gage instrumentation on localized strain responses in AC pavements is evaluated through finite element (FE) simulations. The distinct feature of the developed 3-D FE model is the inclusion of elastic strain gages in viscoelastic AC layers. These strain gages were modeled in both longitudinal and transverse directions at multiple depths within the AC layers. Influencing factors such as pavement temperature, vehicle speed, contact pressure, tire wander, and AC mixture were considered. FE simulations reveal that the inclusion of a strain gage results in considerably lower strain responses than otherwise predicted. This is manifested most at high pavement temperatures, low vehicle speeds, and high contact pressures. The presence of a strain gage may result in a prediction error of up to 73 percent for the conditions and materials considered.

DOI:10.6135/ijprt.org.tw/2013.6(3).225

**Key words:** Finite Element Analysis; Pavement Response; Strain Gage; Viscoelastic.

## Introduction

Mechanistic-empirical design procedures for flexible pavements utilize mechanistic models to predict pavement responses, such as stresses and strains. One of the most important parameters required by the response models is the modulus of each pavement layer. Two basic means of obtaining layer material properties are laboratory and in situ testing. Typical laboratory tests for asphalt concrete (AC) materials include the complex modulus ( $E^*$ ) test, the indirect tensile test (IDT), and tests related to the shear stiffness ( $G^*$ ) measured using the simple shear tester (SST) at low, intermediate, and high test temperatures. The resilient modulus test is performed to determine the moduli of granular materials (e.g., base, subbase, and subgrade). For decades, pavement engineers have worked in the mechanistic-empirical (M-E) design procedures for flexible pavements, the mechanistic response models are used to predict pavement responses: stresses, strains, and deflections. A response model must account for the effects of climate, traffic, material properties, and pavement structure. Historically, mechanistic response models have included layered-elastic and finite element (FE) models. Generally speaking, these approaches have proven reasonably accurate for design purposes. However, there is a need to further validate the response models, particularly with regard to pavement dynamic response. Fortunately, test roads with instrumented response devices such as strain gauges allow for direct measurement of the pavement response. Measured responses from

instrumented pavements may be more reliable than computed responses because all mechanistic response models are based on assumptions that, to some extent, simplify actual field conditions. By measuring the responses directly, the assumptions and simplifications are not of concern. However, the introduction of the instrumentation into the pavement structure may itself inherently and significantly affect the pavement responses. This concern has led to questions about what is actually being measured by in-situ gages. When comparing measured and predicted responses, can one set of information be considered the “ground truth?”

In a prior study [1], a 3-D viscoelastic based finite element (FE) model was developed to capture flexible pavement response to vehicular loading. Partial validation analyses indicated a prediction error varying from 20 to 30 percent from FE simulations as compared to response data collected from strain gages installed in asphalt concrete (AC) layers. A vital assumption in the previous FE model was that AC layers were homogenous continuum media. The work presented here extends the previous work through assessing impact of strain gage instrumentation on localized strain responses in AC layers.

## Characterization of AC Materials

While the behavior of viscoelastic materials, such as AC, is a direct function of the time for which the loading is applied, it is also dependent on the temperature of the material at the time of loading, previous loading history, and the age of the material. Whenever the time dependent response of AC satisfies the requirement of proportionality and superposition, its behavior is termed linear viscoelastic (LVE). Assuming that the materials do not age with time, AC usually shows nonlinear behavior under very extreme conditions, and under most field situations, its behavior is close to

<sup>1</sup> Airport Pavement Research, Gemini Technologies, Inc., Egg Harbor Twp, NJ 08234, USA.

<sup>+</sup> Corresponding Author: E-mail hao.yin@gemitek.com

Note: Submitted March 30, 2012; Revised November 28 2012; Accepted December 5, 2012.

linear.

Mechanistic response models utilize the AC modulus, taking into account the range of temperatures and loading rates expected in the field. In this study, the complex modulus test, also referred to as Simple Performance Test (SPT), was conducted to determine the elastic modulus of AC materials. The amplitude of the applied uniaxial haversine load is selected based on the material stiffness, temperature (4, 10, 25, and 40°C), and frequency (0.1, 0.5, 1, 5, 10, and 25 Hz) to ensure that the strain response stays within the LVE range [2]. With  $|E^*|$  data from multiple temperatures and loading frequencies, a  $|E^*|$  master curve was then constructed. The master curve describes both the time and temperature dependency of AC materials. Three AC mixtures were included in the study. These mixtures have the same performance grade conventional binders (PG 64-22) but different nominal maximum aggregate sizes (12.5 mm, 19 mm, and 25 mm). Hereafter, these mixtures are referred to as Mixture 1, Mixture 2, and Mixture 3. Dynamic modulus master curves of these mixtures are shown in Fig. 1.

### Strain Gage in AC Pavement

Fundamentally, all strain gages are designed to convert mechanical motion into an electronic signal. A change in capacitance, inductance, or resistance is proportional to the strain experienced by the sensor. If a wire is held under tension, it gets slightly longer and its cross-sectional area is reduced. This changes its resistance (R) in proportion to the strain sensitivity (S) of the wire's resistance. When a strain is introduced, the strain sensitivity, which is also called the gage factor (GF), is given by:

$$GF = \Delta R / S \tag{1}$$

If the gage factor were due entirely to dimensional change, Poisson's ratio would suggest that the gage factor for any wire would be approximately 1.7 [3]. However, different types of strain gages with different gage factors are commercially available, each having been developed in response to a demand for a gage to meet or withstand specific conditions.

In this study, a typical H-type AC strain gage was modeled for dynamic strain measurements because of its success in earlier flexible pavement instrumentation projects [4-7]. The gage is 102mm in length with 75mm wide arms, as illustrated in Fig. 2. The gage is a quarter bridge with a resistance of 120ohms, and has a gage factor of 2.0. It has a physical range of up to 1500 microstrains and a thermal range from -30 to 150°C. An elastic modulus of 2.2 GPa was assumed for the gage. The stainless steel arms (for stainless steel, typical elastic modulus is about 29 GPa) are fastened at each end of the mid-section and serve as anchors to the pavement. The gage produces a strain measurement when the mid-section is compressed or elongated. Therefore, when the AC is subjected to a force, the mid-section follows any deformation in the material and gives a measurement of strain.

### Finite Element Model

Although theoretical calculations using layered theory are relatively inexpensive and easy, typical assumptions, such as linear elastic

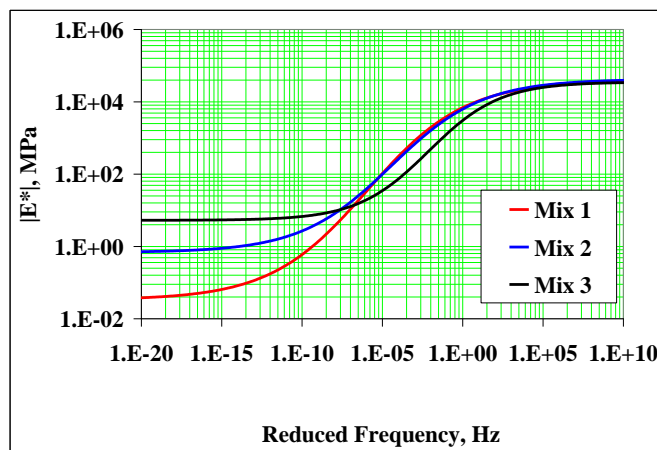


Fig. 1. Dynamic Modulus Master Curves.

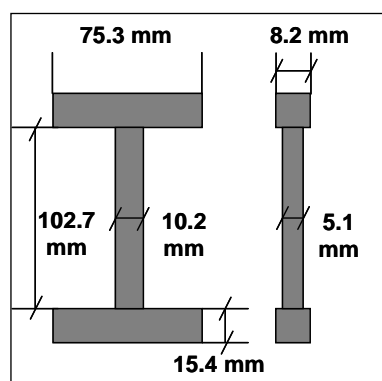


Fig. 2. Dimensions of Modeled AC Strain Gage.

response of AC materials and circular contact area, can significantly affect the reliability of analysis results. Hence, an advanced theoretical analysis tool, such as the finite element method (FEM), would be needed. The FEM is by far the most universally applicable numerical technique for flexible pavements [8]. It provides a modeling alternative that is well suited for applications involving pavement systems with inelastic materials, unusual boundary constraints or complex loading conditions. The general purpose finite element software ABAQUS version 6.6 [9] was used in this study for FE modeling of the pavement structure. The following sections highlight some features of the developed FE model.

### Model Geometry and Boundary Conditions

Different gage orientations (longitudinal and transverse) demand a 3-D FE model. Due to the double symmetry of the geometry and load about the horizontal x and y axes, only a quarter model is need. The developed symmetric 1/4 3-D FE model is 2000 mm in length, 1000 mm in width, and 1500 mm in height. These dimensions were selected to reduce any edge effects, while keeping the element size within acceptable limits. The developed FE model represents a conventional flexible pavement section with three layers, AC, granular base, and subgrade. The AC strain gage was arbitrarily placed at depths of 50 mm, 100 mm, 150 mm, 200 mm, 250 mm, and 300 mm in both longitudinal and transverse directions. The bottom of the model was prevented from axial movements in the three directions to represent the bedrock (rigid layer) beneath the

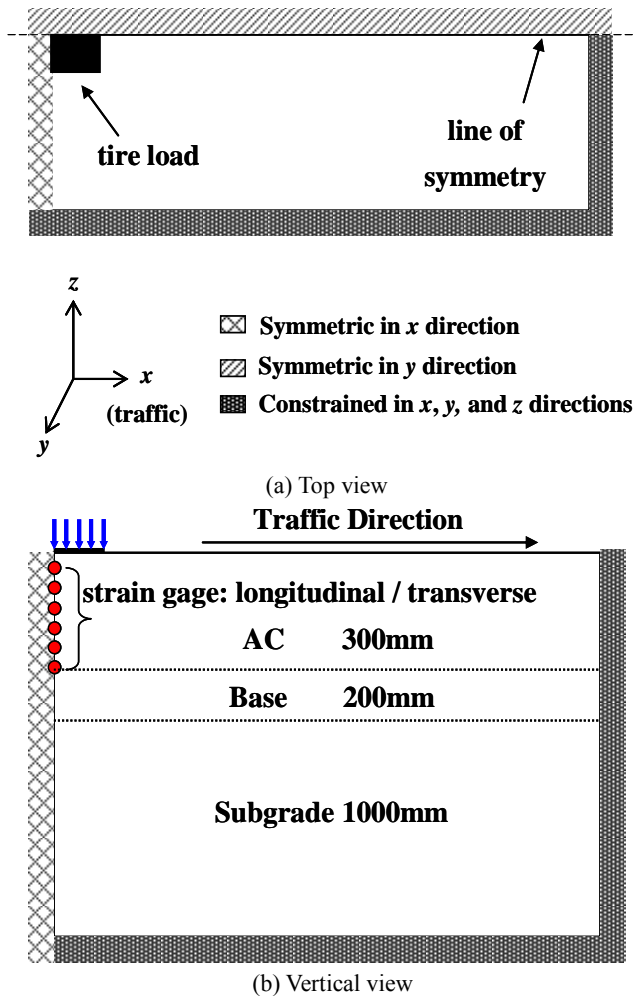


Fig. 3. Boundary Conditions.

pavement structure, as demonstrated in Fig. 3. Zaghoul and White [10] and Kuo et al. [11] have successfully adopted such boundary conditions. Strain gage and AC materials were considered perfectly bonded to one another so that the nodes at the interface had the same displacement in all three ( $x$ ,  $y$ ,  $z$ ) directions. This bonding treatment represents the best interface condition that can be achieved during field instrumentations.

### Material Properties

In this study, pavement materials are considered in two general categories: viscoelastic material (AC) and elastic materials (granular subbase and subgrade, and strain gage). ABAQUS assumes that the viscoelastic material is defined by a Prony series expansion of the dimensionless relaxation modulus. However, owing to experimental constraints such as limitation of machine loading capacity, the relaxation modulus test is rarely conducted in the laboratory. Therefore, a numerical method [12] was used to obtain the relaxation modulus indirectly from the dynamic modulus data. By applying the specific temperature as a boundary condition, the relaxation modulus master curve was shifted from a reference temperature (i.e., 25°C) to the specific temperature of interest (e.g., 40°C) through a Quasi-static analysis procedure.

Granular materials are not elastic and result in permanent

deformation under stationary loads. However, under the repeated application of typical moving traffic loads, most of the deformations are recoverable and can be considered elastic [13]. Elastic modulus values of 500 MPa and 200 MPa were assigned to the subbase and subgrade layers in the FE model, respectively. These moduli represent typical granular materials' stiffnesses in Pennsylvania. The strain gage was also modeled in a linear elastic mode with assumed values of Poisson's ratio 0.30 and 0.20 for the stainless steel (anchors) and the mid-section, respectively.

### Vehicular Load

To accurately simulate pavement response to vehicular loading, the dimensions of the contact area between the tire and pavement are required. Experimental measurements have shown that the actual loading conditions are non-uniform and depend on the tire construction, tire load and tire inflation pressure [14]. This nonuniform pressure might result due to the stiffening effect of the tire wall. Luo and Prozzi [15] investigated the effect of the difference between the modeled uniform and the actual distributed pressures on the pavement distress, especially top-down cracking. The authors observed the most significant difference at the pavement surface. Since it is well documented that the difference in the tire print area configuration is insignificant at greater depths, it was believed that applying a uniform contact pressure over a rectangular tire print area would be acceptable for strain predictions at depths greater than 50mm. A single uniform contact pressure was applied on a rectangular area (330 mm x 220 mm) of the surface of developed FE model.

Quasi-static analysis procedures were used to simulate the field scenario where the moving load approaches and leaves the area of interest. The effect of a moving load on a point in the pavement is simulated by noting that a time function of the stress can be used to approximate the stress experienced by the point. The relationship between the duration of moving load and the load amplitude was approximated through a sine function presented by Huang [13]. Load pulses from various vehicle speeds were simulated assuming that the duration of the load pulse does not vary through the pavement depth. However, this assumption is not strictly true for actual pavement [16, 17].

### Element Type

In this study, one of the main challenges related to the finite element modeling is the quality (the degree) of adhesion between two very different components, soft material (AC) and hard material (strain gage assembly). If two materials do not adhere well to each other, the predicted pavement response at the center of the mid-section of the strain gage can be seriously affected (Fig. 5a). Although the 8-node hexahedral element is the most common element used in 3-D FE modeling, a complex solid model/interface, as the case in this study, can be decomposed into tetrahedral elements more easily when compared to hexahedral elements. To improve the rate of convergence and the compatibility at the AC material – strain gage (SG) interface, 10-node quadratic tetrahedron elements were used (Fig. 5b). Considering the temperature dependency of AC materials,

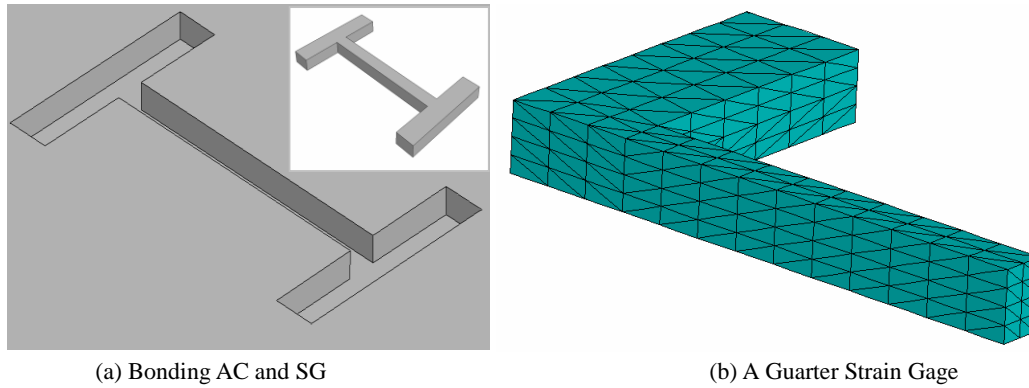


Fig. 4. Modeling AC-SG Interface.

Table 1. Elastic Properties Used in Mesh Refinement Analysis.

Layer	Thickness, mm	Elastic Modulus, MPa	Poisson's Ratio
AC	300	2000	0.35
Base	200	500	0.4
Subgrade	1500	200	0.5

coupled temperature-displacement features that have both displacement and temperature degrees of freedom were also added into elements.

**Element Size**

Element size needs to be carefully selected since it directly affects the level of accuracy obtained from the FE model. Computational time and data storage space also need to be considered for the desired level of accuracy. To determine the optimum element size, each pavement layer was first meshed with large elements. The element mesh was continuously refined until the vertical stress continuity at the layer interface was obtained. During this mesh refinement process, linear elastic response of pavement materials was assumed, as listed in Table 1. A contact pressure of 600 kPa was uniformly applied over a rectangular tire print area on the pavement

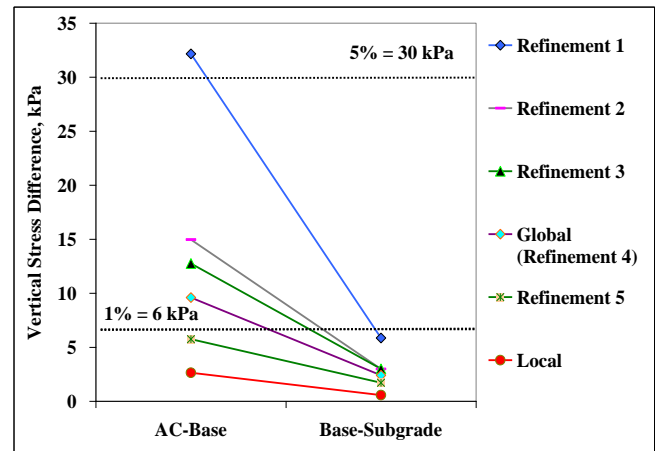


Fig. 5. Determination of the Optimum Element Size.

surface.

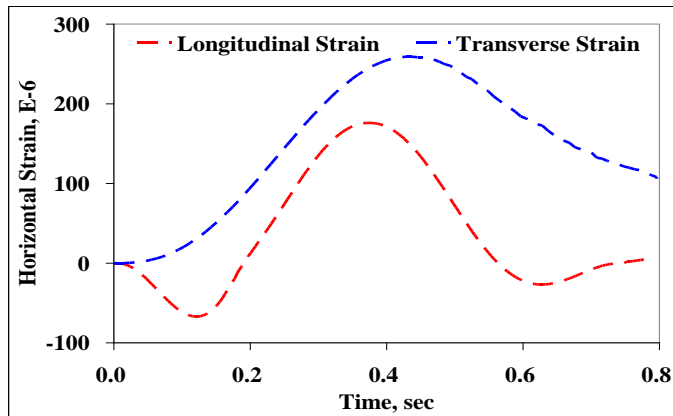
The impact of the mesh size was evaluated at the points along the vertical axis at the center of the loaded area. Table 2 summarizes the vertical stress differences for different mesh refinements. A graphic comparison of different mesh refinements is shown in Fig. 6. It can be seen that the continuity of vertical stresses at a layer interface is highly affected by the element size of the upper layer. With an

Table 2. Mesh Refinement Analysis Results.

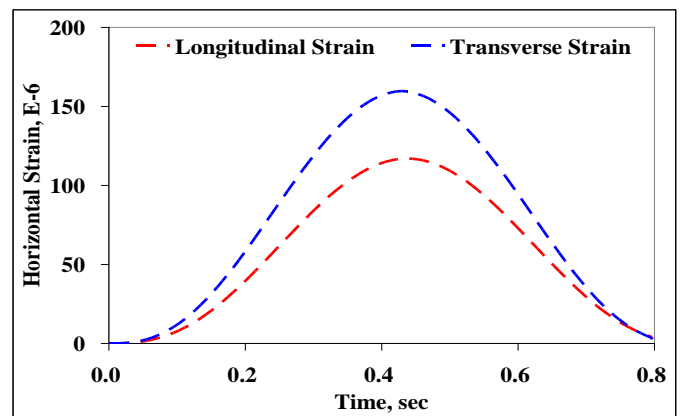
Mesh Refinement	Layer	Element Size, mm	Number of Elements	Output File Size, Mbytes	Computational Time, sec	Vertical Stress Difference at Layer Interface, kPa	
1	AC	50	7760	14.5	44	AC-Base	32.2
	Base	50				Base-Subgrade	5.9
	Subgrade	50					
2	AC	25	35235	79.8	236	AC-Base	15
	Base	25				Base-Subgrade	3
	Subgrade	25					
3	AC	20	52272	126.3	328	AC-Base	12.7
	Base	20				Base-Subgrade	3
	Subgrade	25					
4 (global)	AC	10	97809	270.2	958	AC-Base	9.6
	Base	20				Base-Subgrade	2.4
	Subgrade	20					
5	AC	10	211680	766.7	20880	AC-Base	5.8
	Base	10				Base-Subgrade	1.7
	Subgrade	20					

**Table 3.** Mesh Refinement Analysis Results from Global-Local FEM Approach.

Mesh Refinement	Layer	Element Size, mm	Number of Elements	Output File Size, Mbytes	Computational Time, Sec	Vertical Stress Difference at Layer Interface, kPa	
6 (local)	AC	5	66480	194.4	640	AC-Base 2.6	Base-Subgrade 0.6
	Base	5					
	Subgrade	20					



(a) Without Strain Gage



(b) With Strain Gage

**Fig. 6.** Typical Pavement Responses at 50 mm Depth (Mix 2, Pavement Temperature = 40°C, Vehicle Speed = 8 kph, Contact Pressure = 800 kPa).

element size of 10 mm for AC and base layers, and 20 mm for subgrade, the stress difference is reduced to about 1 percent of applied tire load, 6 kPa. However, the required computational time and data storage space are very high for this level of solution accuracy. Therefore, the Global-Local FEM approach was further implemented in the mesh refinement analysis. This approach utilizes the cut-boundary displacement method, also known as the specified boundary displacement method, which is very efficient in terms of computing and hardware requirements [1, 18-20]. It also enables users to experiment with different designs (e.g., finer meshes) for the region of interest [21]. An example of using mesh refinement 4 (Table 2) as the global model is presented in Table 3. Convergence results from this Global-Local approach suggests that running FE models in this fashion can dramatically reduce computational time and data storage space, while keeping an excellent level of solution accuracy. This approach makes it possible to model the strain gage more efficiently.

### Typical Pavement Dynamic Response

For demonstration purposes, pavement responses predicted from some of the FE simulations are shown in Fig. 7. For both scenarios (without and with strain gage), the peak value of transverse strain is always higher than that of longitudinal strain. This observation agrees with findings reported by Huhtala and Pihlajamaki [22]. Response curve at different depths exhibits a similar shape although the strain magnitude changes with pavement depth, vehicle speeds, pavement temperature, and contact pressure.

### Response without Strain Gage

In general, the response curve (Fig. 7a) suggests that the FE model

without strain gage is capable of simulating the viscoelastic behavior of AC materials, such as the time retardation, as well as the response relaxation. Several observations may be drawn from Fig. 7a. The longitudinal strain always reaches its peak value before the transverse strain. For longitudinal strain, there is always compression (negative strains) first, then tension (positive strains) when the load is directly on top of the strain gage, and subsequently compression. An explanation of the compressive strain in the longitudinal direction is that the vertical acceleration of a point within the pavement changes from positive to negative as the loading axle passes over it [23]. The compressive strain in the longitudinal direction may be also related to the combination of bending stresses and horizontal shear stresses. However, transverse strain is always in tension regardless of the relative position of tire load to the strain gage (tire wander). It is also worth noting that longitudinal strain recovers rapidly so that very little permanent deformation occurs. However, if the next pass of tire load comes before the complete relaxation of transverse strain has taken place; the unrecovered inelastic (residual) strain in the transverse direction may cause permanent deformation, especially at shallow depths.

### Response with Strain Gage

Compared to the FE model without strain gage, inclusion of a strain gage always results in predicting smaller strain responses. The time retardation of the viscoelastic behavior of AC materials is not present in Fig. 7b. The longitudinal and transverse strains reach their peak values at the same time. Finally, the longitudinal strain does not show the compression-tension-compression pattern and the transverse strain does not preserve unrecovered strain at the end of loading time. All of these dissimilarities may result from the elastic behavior of the strain gage.

**Table 4.** Experiment Design for FE Simulations.

Case No.	Pavement Temperature, °C	Vehicle Speed, kph	Contact Pressure, kPa	Tire Wander, mm	AC Mix
1	20	48	600	0	2
2	40	48	600	0	2
3	0	48	600	0	2
4	20	8	600	0	2
5	20	96	600	0	2
6	20	48	800	0	2
7	20	48	400	0	2
8	20	48	600	110	2
9	20	48	600	220	2
10	20	48	600	0	1
11	20	48	600	0	3

### Evaluation of Strain Response

As presented in the previous section, strain responses are sensitive to the presence of the strain gage. Since AC relaxes over time and dissipates energy upon unloading due to its viscoelastic nature, both tensile and compressive strains contribute to the overall damage of the pavement, as observed for the case of no strain gages. On the other hand, no compressive strain is observed for the pavement with strain gage.

To evaluate the effects of inclusion of an elastic mode strain gage on pavement response, it is reasonable to compare the peak horizontal strain values in both longitudinal and transverse directions. Consequently, an experiment considering various factors affecting pavement response was designed, as illustrated in Table 4. Case 1 was considered as the reference case for response evaluations.

Since actual pavement response is represented by the case of no strain gages, the prediction error in percentage,  $e$ , is calculated as:

$$e = \frac{R_{WSG} - R_{WOSG}}{R_{WOSG}} * 100 \quad (2)$$

where  $R_{WOSG}$  is the peak response simulated from FE models without strain gages and  $R_{WSG}$  is the peak response simulated from FE models with strain gages. A positive value of  $e$  indicates an overprediction from FE simulations, while a negative value of  $e$  suggests an underprediction. This error will be further discussed as presented in Table 5.

### Effect of Pavement Temperature on Strain Responses

The effect of pavement temperature on pavement response was evaluated for Cases 1, 2, and 3 as given in Table 4. Longitudinal and transverse strain responses predicted from these FE simulations are summarized in Table 5. In general, a pavement temperature change from moderate (20°C) to high (40°C) results in a more significant jump in the magnitude of both longitudinal and transverse strains than that from a low (0°C) to moderate temperature change. An interesting observation from Table 4 is the occurrence of a compression-tension transition in longitudinal strains. The depth at which this transition occurs decreases as the pavement temperature increases. The transition occurs at a depth between 50 and 100 mm for moderate and low temperatures while at less than 50 mm for the high temperature. One possible explanation of this observation is that the bending of the upper AC layer is condensed due to the loss of AC stiffness at the high temperature. On the other hand, transverse strains are always in tension regardless of pavement temperature. Transverse strains typically have a larger magnitude than longitudinal strains. The magnitudes of these two strains are quite close at the low temperature and deeper locations.

Except for the high temperature, the prediction error is normally decreases along with pavement depths. Negative average  $e$  values

**Table 5.** Pavement Responses at Different Pavement Temperatures.

Pavement Temperature, °C	Depth, mm	Longitudinal Strain, E-6			Transverse Strain, E-6		
		Without SG	With SG	$e$ , %	Without SG	With SG	$e$ , %
40	50	111	45	-60	192	80	-58
	100	259	132	-49	391	175	-55
	150	234	120	-49	319	130	-59
	200	192	94	-51	242	120	-51
	250	156	89	-43	187	96	-49
	300	148	72	-51	147	70	-52
20	50	-22	-10	-52	17	9	-47
	100	17	11	-40	30	17	-44
	150	36	25	-32	44	27	-38
	200	49	39	-19	55	46	-16
	250	56	48	-14	61	52	-14
	300	63	60	-5	76	69	-9
0	50	-7	-5	-35	2	1	-27
	100	7	6	-14	7	6	-14
	150	12	10	-17	13	11	-15
	200	16	14	-13	18	16	-8
	250	20	18	-11	21	20	-5
	300	24	24	-2	23	23	-3

**Table 6.** Pavement Responses at Different Vehicle Speeds.

Vehicle Speed, kph	Depth, mm	Longitudinal Strain, E-6			Transverse Strain, E-6		
		Without SG	With SG	$e, \%$	Without SG	With SG	$e, \%$
8	50	-29	-12	-58	49	18	-63
	100	43	17	-60	75	26	-65
	150	76	30	-61	89	42	-53
	200	95	47	-51	115	59	-49
	250	111	72	-35	146	69	-53
	300	136	88	-36	178	98	-45
48	50	-22	-10	-52	17	9	-47
	100	17	11	-40	30	17	-44
	150	36	25	-32	44	27	-38
	200	49	39	-19	55	46	-16
	250	56	48	-14	61	52	-14
	300	63	60	-5	76	69	-9
96	50	-3	-3	-24	7	6	-19
	100	11	8	-21	14	12	-17
	150	16	13	-16	19	16	-16
	200	19	17	-9	27	23	-15
	250	23	21	-7	27	24	-12
	300	33	31	-4	34	32	-6

indicate that the presence of a strain gage dramatically underpredicts pavement responses, particularly at high temperature. The elevated prediction error is perhaps the result of large difference between moduli of AC materials and strain gage. At high temperatures, AC materials experience a creep deformation due to viscous flow. Yet, this deformation is constrained by the strain gage because of its significantly higher elastic modulus. This constraint creates prediction errors up to -50 percent and -54 percent for longitudinal and transverse strains, respectively. When the pavement temperature drops, AC materials become stiffer and more brittle. At low temperatures, the modulus of asphalt concrete approaches to that of elastic modulus of the strain gage. Consequently, only -15 percent and -12 percent average prediction errors are observed for longitudinal and transverse strains, respectively.

### Effect of Vehicle Speed on Strain Responses

Due to the time-dependent behavior of AC materials, higher strains are expected as the vehicle speed is reduced (slow loading rate). The effect of vehicle speed on pavement response is clear from Table 6. These responses were predicted from Cases 1, 4, and 5 of Table 4. The speed effect is more dominant at lower speeds (e.g. 8 kph) and deeper locations. Considerable difference is observed when the speed is increased from 8 kph to 48 kph. However, there is not a significant change in response when the speed is increased from 48 kph to 96 kph. Various research works [24-26] have shown that a significant reduction in the measured strains was observed as a result of increasing the vehicle speeds.

The reduction in prediction errors at deeper locations is more evident for moderate and high speeds (48 and 96 kph). Average  $e$  values reveal the presence of a strain gage distinctly affects pavement responses, particularly at lower vehicle speeds. For a moderate temperature (20°C), high  $e$  values (-50 to -55 percent) are observed at a vehicle speed of 8kph. Low vehicle speed (slow

loading rate) tends to reduce stiffness of the AC material; thus a larger deformation would be expected. However, this tendency for larger deformation faces resistance by the strain gage with higher elastic modulus. At high vehicle speeds (fast loading rates), asphalt concrete manifests a more rigid behavior with its modulus becoming closer to the elastic modulus of the strain gage. Hence, the constraint imposed by the strain gage at higher speeds is not as great as at lower speeds. At the highest vehicle speed (96 kph), the average prediction errors are about -13 percent and -14 percent for longitudinal and transverse strains, respectively.

### Effect of Contact Pressure on Strain Responses

Strain responses predicted for Cases 1, 6, and 7 of Table 4 are summarized in Table 7. At a moderate pavement temperature (20°C) and vehicle speed (48 kph), the effect of contact pressure on pavement responses is only considerable at the bottom of the AC layer. This characteristic is observed in both longitudinal and transverse strains. The level of contact pressure does not substantially influence prediction errors. It is noticed that the prediction errors for both longitudinal and transverse strains reach their peak values at a depth less than 100 mm and then begin falling rapidly at deeper locations.

### Effect of Tire Wander on Strain Responses

One important factor that should be considered in the pavement response evaluation is the lateral position of the vehicle load (tire wander). FE simulation results for Cases 1, 8, and 9 of Table 4 are presented in this subsection. Two different magnitudes, 110 and 220 mm, were considered for wander in this analysis. These two values correspond to a half-width and one full width of the used rectangular tire print area, respectively. As shown in Table 8, the larger the lateral deviation of the tire from the gage, the less the

**Table 7.** Pavement Responses for Different Contact Pressures.

Contact Pressure, kPa	Depth, mm	Longitudinal Strain, E-6			Transverse Strain, E-6		
		Without SG	With SG	$e, \%$	Without SG	With SG	$e, \%$
800	50	-21	-7	-68	19	6	-68
	100	20	3	-84	39	11	-73
	150	40	16	-59	58	31	-47
	200	59	47	-20	73	68	-7
	250	85	79	-7	102	98	-4
	300	100	95	-5	121	119	-2
600	50	-22	-10	-52	17	9	-47
	100	17	11	-40	30	17	-44
	150	36	25	-32	44	27	-38
	200	49	39	-19	55	46	-16
	250	56	48	-14	61	52	-14
	300	63	60	-5	76	69	-9
400	50	-5	-3	-28	2	1	-23
	100	3	2	-33	7	3	-55
	150	13	8	-39	10	6	-40
	200	18	13	-26	18	14	-23
	250	34	32	-6	30	28	-8
	300	42	40	-5	40	37	-9

**Table 8.** Pavement Responses for Different Tire Wanders.

Tire Wander, mm	Depth, mm	Longitudinal Strain, E-6			Transverse Strain, E-6		
		Without SG	With SG	$e, \%$	Without SG	With SG	$e, \%$
0	50	-22	-10	-52	17	9	-47
	100	17	11	-40	30	17	-44
	150	36	25	-32	44	27	-38
	200	49	39	-19	55	46	-16
	250	56	48	-14	61	52	-14
	300	63	60	-5	76	69	-9
110	50	-10	-7	-29	9	6	-28
	100	-4	-3	-24	14	12	-15
	150	10	9	-10	17	13	-24
	200	18	16	-14	32	24	-25
	250	31	28	-8	43	34	-22
	300	50	44	-13	60	53	-12
220	50	-25	-17	-32	3	2	-27
	100	-17	-14	-19	10	8	-16
	150	-10	-8	-22	13	12	-13
	200	3	3	-19	21	17	-16
	250	12	10	-15	25	21	-18
	300	20	18	-12	27	23	-13

magnitude of the strain response is expected to be. This feature is manifested at deeper locations. It should also be noted that the lateral position of the vehicle tire has a large impact on the compression-tension transition in longitudinal strains. As the tire load moves away from the gage, the neutral axes moves downward. This observation is primarily caused by the bending of the AC layer. At smaller depths, a substantial reduction in prediction errors is observed when the load is moved laterally from 0 mm to 110 mm. Nevertheless, there is not a significant change in  $e$  values when the load is moved from 110 mm to 220 mm.

### Effect of Mixtures on Strain Response

Table 9 lists strain responses predicted from Cases 1, 10, and 11 of Table 4. Similar strain responses were predicted from three AC mixtures. Slight variations are observed in prediction errors between Mixtures 1, 2, and 3. Since only one pavement temperature (20°C) and vehicle speed (48 kph) were considered, further research on this subject is needed to strengthen the conclusions.

### Concluding Remarks

Although instrumentation has become a promising tool for quantitative measurement of pavement response under true field conditions, there has been a concern among pavement engineering

**Table 9.** Pavement Responses for Different Mixtures.

AC Mixture	Depth, mm	Longitudinal Strain, E-6			Transverse Strain, E-6		
		Without SG	With SG	$\epsilon$ , %	Without SG	With SG	$\epsilon$ , %
1	50	-18	-10	-41	4	3	-37
	100	9	7	-22	11	9	-17
	150	18	15	-17	16	13	-21
	200	24	18	-26	30	23	-22
	250	55	44	-20	65	57	-13
	300	67	51	-24	81	68	-16
2	50	-22	-10	-52	17	9	-47
	100	17	11	-40	30	17	-44
	150	36	25	-32	44	27	-38
	200	49	39	-19	55	46	-16
	250	56	48	-14	61	52	-14
	300	63	60	-5	76	69	-9
3	50	-16	-10	-39	5	2	-46
	100	16	13	-19	13	8	-38
	150	27	23	-15	20	16	-16
	200	30	25	-16	38	27	-27
	250	52	44	-15	42	35	-17
	300	79	69	-13	96	84	-13

community that whether the introduction of the gage into the pavement structure would itself inherently and significantly affect the measured responses. In this paper, a FE model was developed to evaluate the impact of embedded strain gages on localized strain responses in the AC layers. With a three-layer conventional flexible pavement structure, strain gages were modeled in both longitudinal and transverse directions at multiple depths in AC layers. Elastic material properties were assumed for these gages. It was also assumed that AC materials and strain gages were fully bonded. Extensive FE simulations under different loading and environmental conditions revealed that including an elastic strain gage in viscoelastic AC materials results in appreciably lower strain responses. This is manifested at high pavement temperature, low vehicle speed, and high contact pressure. The presence of a strain gage may result in a prediction error up to -73 percent.

### Acknowledgements/Disclaimer

The author would like to thank Dr. Shelley Stoffels and Dr. Mansour Solaimanian from The Pennsylvania State University for their technical comments.

### References

1. Yin, H., Stoffels, S., and Solaimanian, M. (2008). Optimization of Asphalt Pavement Modeling based on the Global-Local 3D FEM Approach. *Road Materials and Pavements Design*, 9(2), pp. 345-355.
2. Solaimanian, M., Stoffels, S.M., Hunter, D.A., Morian, D., Sadavisam, S., and Yin, H. (2006). Detailed Final Report for Superpave In-Situ Stress/Strain Investigation. Pennsylvania Transportation Institute, PA, USA.
3. Omega Press LLC, (1996). *The Pressure, Strain, and Force Handbook*, OMEGA Engineering, Inc., Stamford, Connecticut, USA.
4. Baker, H.B., Buth, M.R., and Van Deusen, D.A. (1994). Minnesota Road Research Project: Load Response Instrumentation Installation and Testing Procedures. Final Report, 1992-94, *Report No. MN/PR-94/01*, Minnesota Dept. of Transportation, Maplewood, MN, USA.
5. Sargand, S.M., Green, R., and Khoury, I. (1997). Instrumentation Ohio Test Pavement. *Transportation Research Record*, No. 1596, pp. 23-30.
6. Loulizi, A., Al-Qadi, I.L., Lahouar, S., and Freeman, T.E. (2001). Data Collection and Management of the Instrumented Smart Road Flexible Pavement Sections. *Transportation Research Record*, No. 1769, pp. 142-151.
7. Timm, D.H., Priest, A.L., and McEwen, T.V. (2004). Design and Instrumentation of the Structural Pavement Experiment at The NCAT Test Track. *NCAT Report 04-01*, National Center for Asphalt Technology, Auburn University, Auburn, AL, USA.
8. ERES Consultants Division (2004). Guide for mechanistic-empirical design of new and rehabilitated pavement structures. Final Report NCHRP 1-37A, Champaign, IL, USA.
9. ABAQUS/Standard User's Manual (2002). Finite Element Computer Program. Hibbitt, Karlsson and Sorenson, Inc., Pawtucket, RI, USA, Version 6.3.
10. Zaghoul, S.M. and White, T.D (1993). Use of a three-dimensional, dynamic finite element program for analysis of flexible pavement. *Transportation Research Record*, No. 1388, pp. 60-69.
11. Kuo, M.C., Hall, K.T., and Darter, M. (1995). Three-dimensional finite element model for analysis of concrete pavement support. *Transportation Research Record*, No. 1505, pp. 119-127.
12. Schapery, R. and Park, S. (1999). Methods of Interconversion

- Between Linear Viscoelastic Material Functions. Part II – An Approximate Analytical Method. *International Journal of Solids and Structures*, Vol. 36, pp. 1677-1699
13. Huang, Y. (1993). *Pavement Analysis and Design*. Prentice Hall, NJ, USA.
  14. De Beer, M. (1996). Measurement of Tyre/Pavement Interface Stresses under Moving Wheel Loads. *International Journal of Vehicle Design*, Vol. 3, pp. 97-115.
  15. Luo, R. and Prozzi, J. (2005). Evaluation of the Joint Effect of Wheel Load and Tire Pressure on Pavement Performance. Center for Transportation Research, University of Texas at Austin, TX, USA.
  16. AASHO (1962). The AASHO Road Test: Report 6 – Special Studies. *HRB Spec. Report 61F*, Highway Research Board, Washington, D.C., USA.
  17. Yin, H., Solaimanian, M., Kumar, T., and Stoffels, S. (2007). The Effect of Loading Time on Flexible Pavement Dynamic Response, *A Finite Element Analysis. Mechanics of Time-Dependent Materials*, 11(3-4), pp 265-288.
  18. Whitcomb, J.D. and Woo, K. (1993). Application of iterative global/local finite element analysis, Part 1: Linear analysis. *Communications in Numerical Methods in Engineering*, Vol. 9, pp. 745-756.
  19. Cormier, N.G., Smallwood, B.S., Sinclair, G.B., and Meda, G. (1999). Aggressive submodelling of stress concentrations. *International Journal for Numerical Methods in Engineering*, 46(6), pp. 889-909.
  20. Colombo, D., Giglio, M., and Manes, A. (2007). 3D fatigue crack propagation analysis of a helicopter component. *International Journal of Materials and Product Technology*, 30(1/2/3), pp. 107-123.
  21. Fagan, M.J. (1992). *Finite Element Analysis: Theory and Practice*. John Wiley, New York, USA.
  22. Huhtala, M., Pihlajamaki, J. (1992). Strain and stress measurements in pavements. *Proceedings, Road and Airport Pavement Response Monitoring Systems, No. 22*, ASCE, West Lebanon, New Hampshire, USA, pp. 229-243.
  23. Sebaaly, P.E. and Mamlouk, M. (1987). Prediction of Pavement Response to Actual Traffic Loading, *Proceedings of 74th Transportation Research Board Annual Meeting*, Washington, D.C., USA.
  24. Sebaaly, P.E. and Tabatabaee, N. (1991). Field Evaluation of Strain Gauges in Asphalt Concrete Pavements. *Proceedings, Road and Airport Pavement Response Monitoring Systems, No. 24*, ASCE, West Lebanon, New Hampshire, USA, pp. 382-396.
  25. Al-Qudi, I., Elseifi, M., and Yoo, P. (2004). Pavement Damage Due to Different Tire and Vehicle Configurations. Virginia Tech Transportation Institute, VA, USA.
  26. Yin, H. (2007) Integrating Instrumentation Data in Probabilistic Performance Prediction of Flexible Pavements. Ph.D. Dissertation. The Pennsylvania State University, University Park, PA, USA.